nature portfolio

https://doi.org/10.1038/s41560-021-00777-x

Supplementary information

The impact of surface composition on the interfacial energetics and photoelectrochemical properties of $BiVO_4$

Supplementary Information

The Impact of Surface Composition on the Interfacial Energetics and Photoelectrochemical Properties of $BiVO_4$

Dongho Lee,[1,#] Wennie Wang,[2,#] Chenyu Zhou,[3,4,#] Xiao Tong,[3] Mingzhao Liu,[3,*] Giulia Galli,[2,5,6*] and Kyoung-Shin Choi[1,*]

[1]*Department of Chemistry, University of Wisconsin-Madison, Madison, WI 53706, United States*
[2]*Pritzker School of Molecular Engineering, University of Chicago, Chicago, IL 60637, USA*
[3]*Center for Functional Nanomaterials, Brookhaven National Laboratory, Upton, NY 11973, United States*
[4]*Department of Materials Science and Chemical Engineering, Stony Brook University, Stony Brook, NY 11794, United States*
[5]*Department of Chemistry, University of Chicago, Chicago, IL 60637, USA*
[6]*Argonne National Laboratory, Lemont, IL 60439, USA*

[#] These authors contributed equally.

[*] Correspondence and requests for materials should be addressed to M.L. (email: mzliu@bnl.gov), G.G. (email: gagalli@uchicago.edu), and K.-S.C. (email: kschoi@chem.wisc.edu).

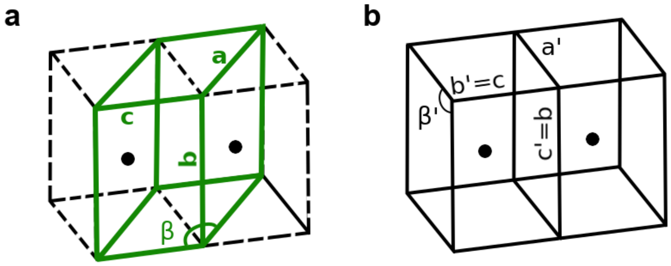

Supplementary Figure 1│ Conversion between C-centered and I-centered monoclinic cells of $BiVO_4$. **a,** a C-centered monoclinic cell (solid green with a, b, c, and β) and **b,** an I-centered monoclinic cell of $BiVO_4$ (solid black with a', b', c', and β'). In **a**, the black dotted lines also represent the I-centered monoclinic cell.[1] The *hkl* indices used in this study are with respect to the C-centered monoclinic cell (C 2/c). We note that in the I-centered monoclinic cell, a' and b' are very similar and β' is close to 90° (a' = 5.1956 Å, b' = 5.0935 Å, c' = 11.7045 Å and β'= 90.383°),[2] which makes it possible to approximate the I-centered monoclinic cell to an I-centered tetragonal cell. Thus, for DFT+U calculations, we used an I-centered tetragonal cell for computational convenience following our previous study;[3] our calculated lattice parameters are a' = b' = 5.172 Å, c' = 11.770 Å.

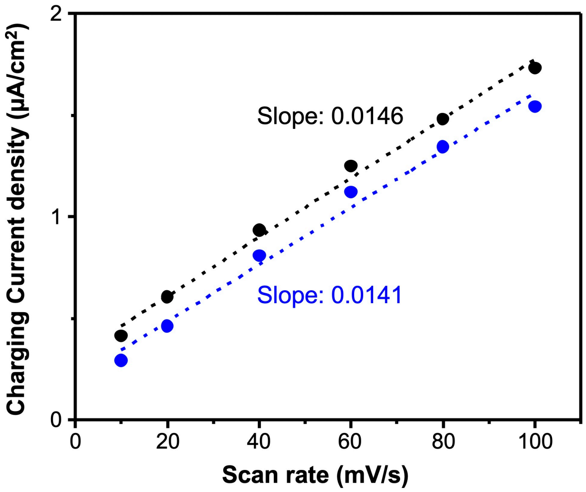

Supplementary Figure 2│ Comparison of electrochemically active surface areas. Electrochemical double layer capacitance measurements of as-prepared (black) and base-treated (blue) $BiVO_4$ electrodes in 0.5 M borate buffer (pH 9.3). Charging current densities were obtained from cyclic voltammograms measured with varying scan rates (10 – 100 mV/s).

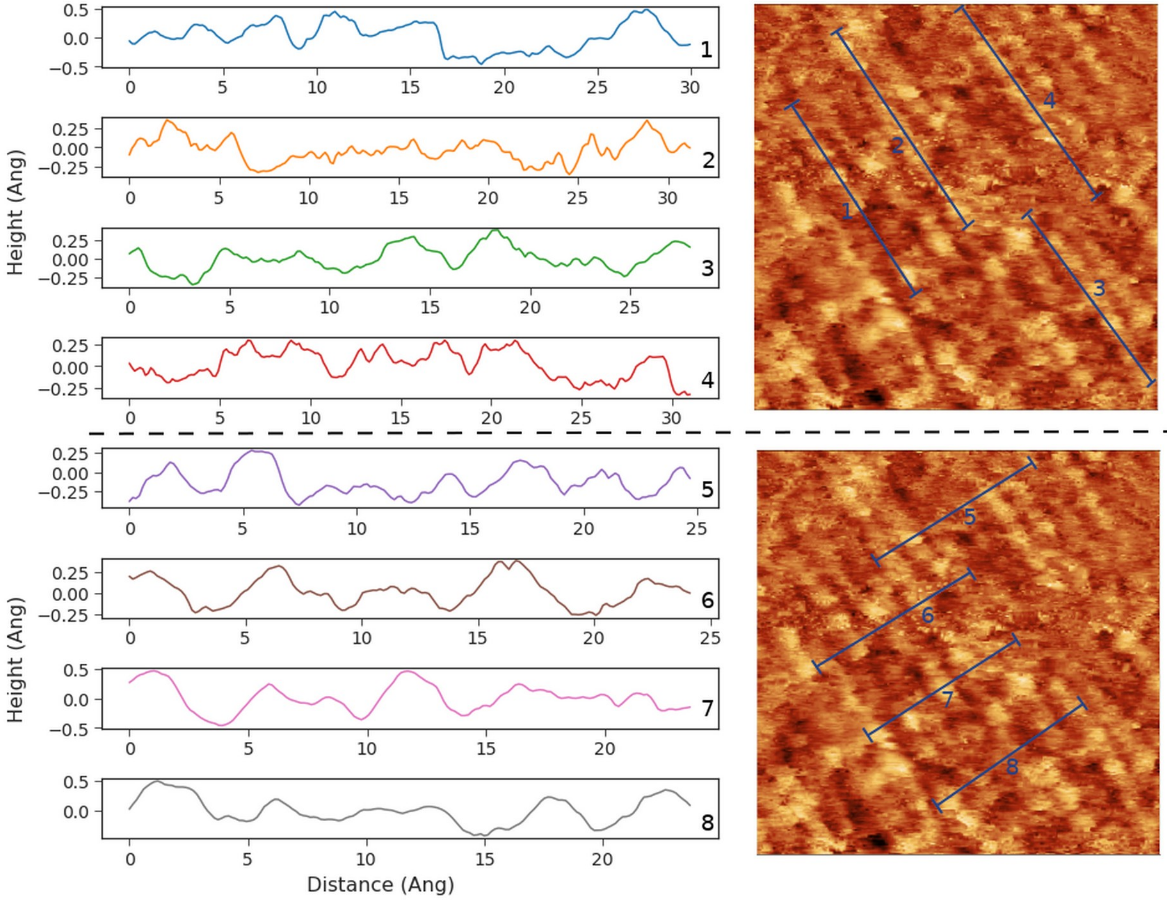

Supplementary Figure 3│ Analysis of the measured STM image (as-prepared sample). Height profiles (left) along the paths shown in the measured STM images (right) of the as-prepared $BiVO_4$ epitaxial sample.

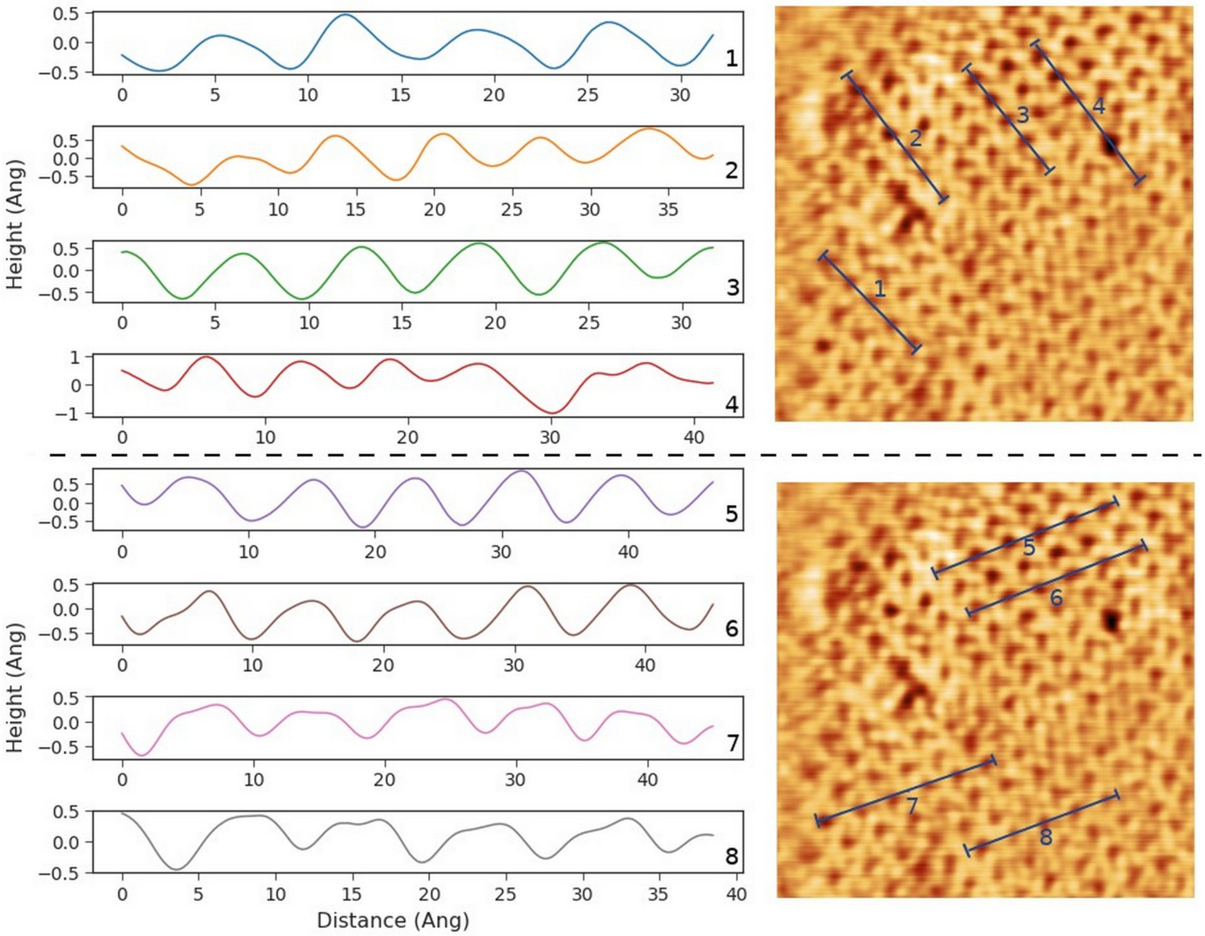

Supplementary Figure 4 | Analysis of the measured STM image (base-treated sample). Height profiles (left) along the paths shown in the measured STM images (right) of the base-treated $BiVO_4$ epitaxial sample.

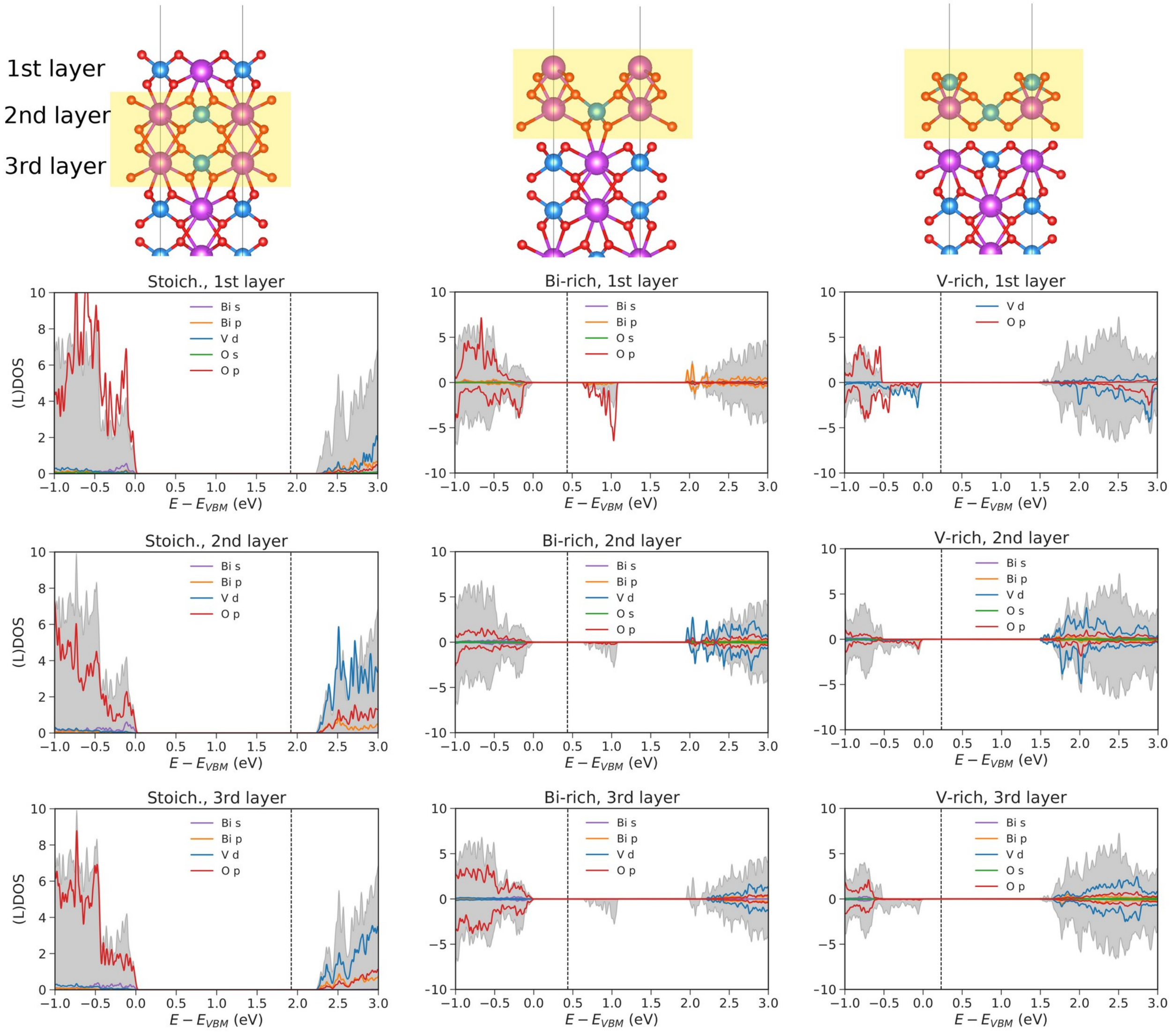

Supplementary Figure 5│ Atom-resolved local density of states (LDOS) of the (010) $BiVO_4$ surface. LDOS for the top three atomic layers from the surface. The stoichiometric (left), Bi-rich (middle), and V-rich (right) surfaces are shown with the atomic layers contributing most to the LDOS at the surface highlighted in yellow boxes. Unlike the Bi-rich and V-rich surfaces, the up and down spin channels of the stoichiometric surface are the same, so only one spin channel is shown. The total DOS is shown as shaded gray regions and scaled by one fifth of the actual DOS for visualization purposes; the Fermi level is denoted with a black dotted line, and the valence band maximum is set to zero in each case.

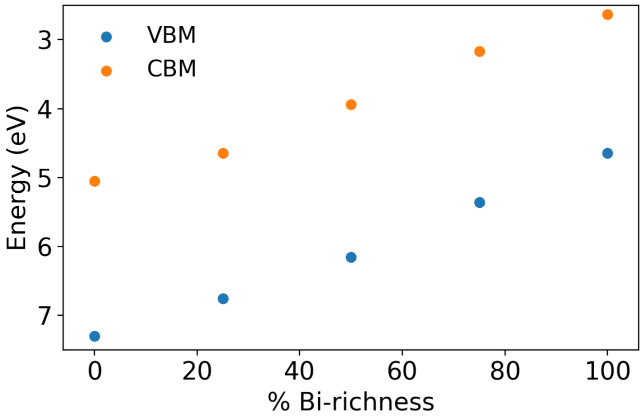

Supplementary Figure 6│ Variation of band alignments with % surface Bi-richness of $BiVO_4$ (010). Alignment of the CBM and VBM with respect to vacuum at various surface Bi-richness compositions. (0% Bi-richness represents the stoichiometric surface, and the Bi-richness increases as the number of V ions removed at the surface increases.) The result shows that as the surface Bi-richness increases, the CBM and VBM shift toward the vacuum level almost linearly. As seen in Supplementary Figure 7, this is largely due to the shift in the average electrostatic potential.

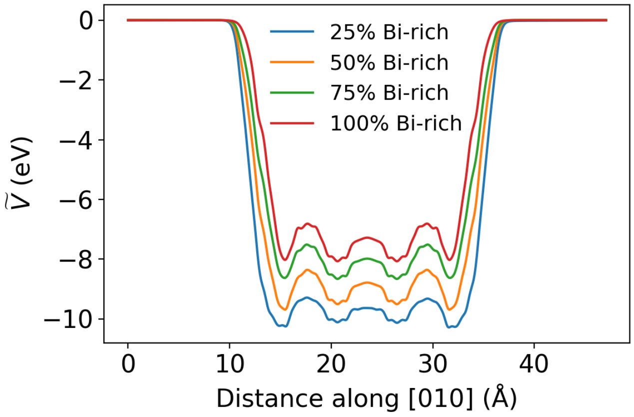

Supplementary Figure 7│ Calculated macroscopic electrostatic potentials ($\tilde{V}$) of $BiVO_4$ (010). Variation of $\tilde{V}$ with surface Bi-richness. The null is vacuum level.

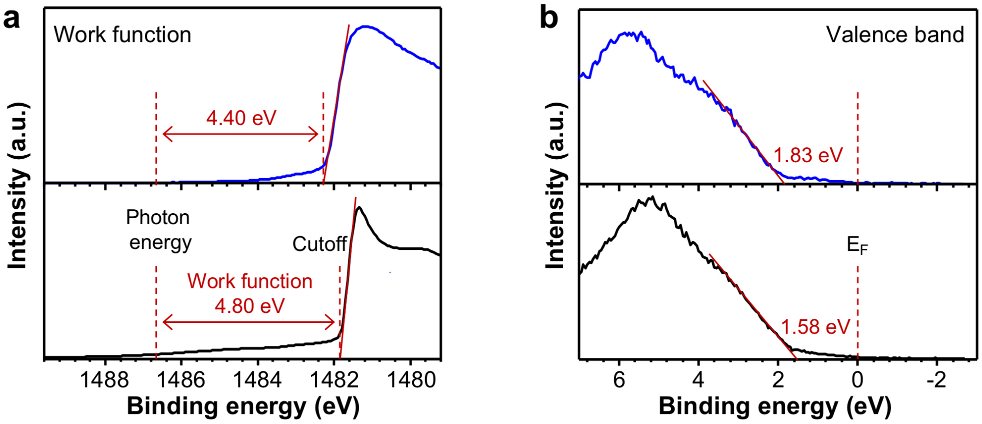

Supplementary Figure 8| XPS spectra of epitaxial BiVO$_4$ (010) electrodes. a, Work function and **b,** valence band (E_F – E_{VBM}) spectra of as-prepared (black) and base-treated (blue) BiVO$_4$ electrodes. Work function was obtained using the following formula: work function = photon energy (1486.68 eV) – secondary electron cutoff.[4]

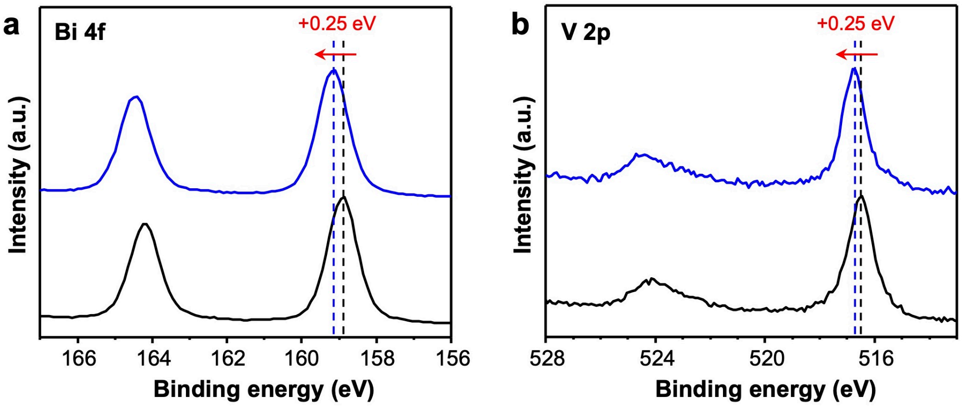

Supplementary Figure 9| Core level XPS spectra of epitaxial BiVO$_4$ (010) electrodes. a, Bi 4f and **b,** V 2p XPS spectra of as-prepared (black) and base-treated (blue) samples. All the core level peaks of the base-treated samples are consistently shifted by +0.25 eV. This is because the binding energy of the core level electrons is measured against the Fermi level of the sample holder, which is equilibrated with the Fermi level of the sample, and the as-prepared and base-treated samples have different Fermi levels.[5] The difference in the Fermi level of the two samples, $\Delta E_F = [E_F\text{(as-prepared sample)} - E_F\text{(base-treated sample)}]$, can be calculated by the equation, $\Delta E_F = \Delta\phi - \Delta\chi$,[5] where $\Delta\phi$ is the difference in the work function and $\Delta\chi$ is the difference in the electron affinity (or the difference in the CBM) of the two samples. As we could not directly measure the CBM by XPS, we used the difference in the VBM as $\Delta\chi$ assuming that the band gaps of the two samples are the same. Since $\Delta\phi$ is 0.4 eV and $\Delta\chi$ is 0.15 eV (**Supplementary Table 1**), ΔE_F is 0.25 eV, meaning that the E_F of the base-treated sample is farther away from the core levels by 0.25 eV. This is why all the core level peaks of the based-treated samples are consistently shifted by +0.25 eV. This also means that this shift is not a chemical shift and that the oxidation states of Bi and V in the two samples are the same and are not affected by the base treatment.

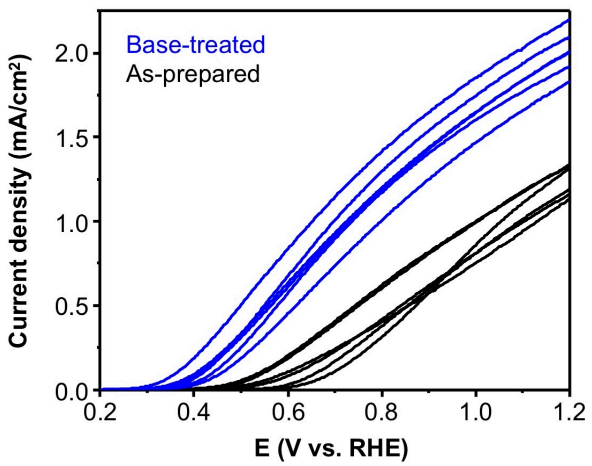

Supplementary Figure 10 | J-V plots obtained from multiple epitaxial $BiVO_4$ (010) electrodes. J-V plots for sulfite oxidation of as-prepared (black) and base-treated (blue) $BiVO_4$ electrodes. Measurements of six different films for each type of sample are shown. The J-V plots shown in Fig. 5a are obtained by averaging six J-V plots shown here for each sample type. The photocurrent was measured in 0.5 M borate buffer (pH 9.3) containing 0.4 M Na_2SO_3 under AM 1.5G, 100 mW/cm^2 illumination.

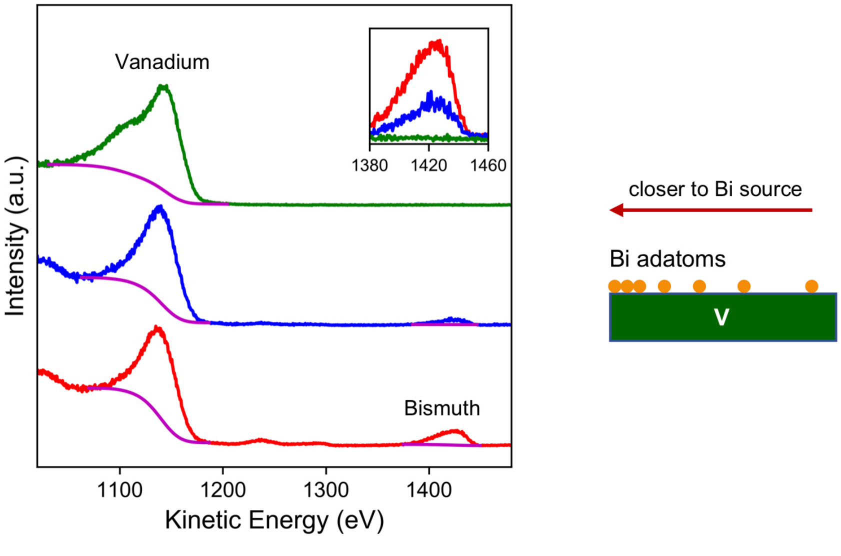

Supplementary Figure 11 | LEIS spectra used to determine the sensitivity factor ratio ρ_V/ρ_{Bi}. LEIS spectra of the Bi/V calibration sample collected at three different spots having different Bi coverages. The inset shows a magnified comparison of the Bi peak regions of the three spectra. The peak areas are calculated by integration after Shirley background subtraction (purple lines). A scheme on the right shows the sample configuration, with the Bi coverage on the V foil increasing from right to left.

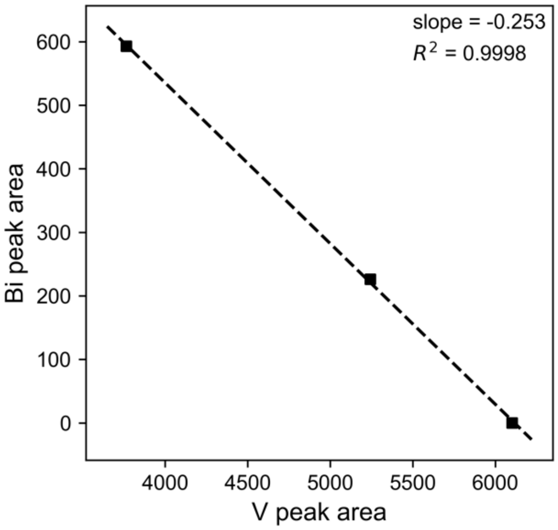

Supplementary Figure 12│ Analysis of the LEIS spectra of the Bi/V calibration sample. The correlation of Bi and V peak areas obtained from the three spots of the Bi/V reference sample with its slope equaling the negative of the sensitivity factor ratio ρ_V/ρ_{Bi}. The dashed line represents the linear regression.

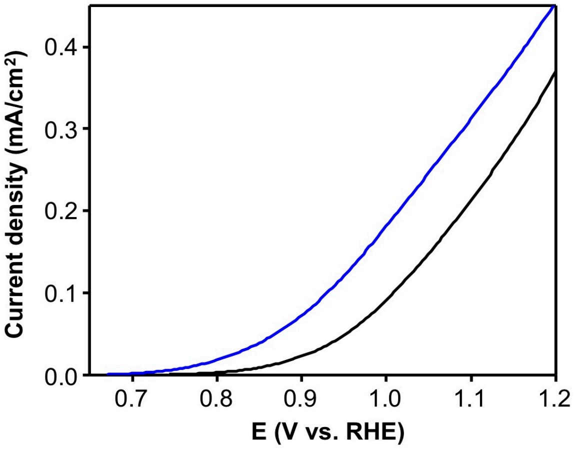

Supplementary Figure 13│ Photoelectrochemical properties of epitaxial $BiVO_4$ (010) electrodes for water oxidation. J-V plots for water oxidation of as-prepared (black) and base-treated (blue) $BiVO_4$ electrodes measured in 0.5 M borate buffer (pH 9.3) under AM 1.5G, 100 mW/cm^2 illumination. The photocurrents for water oxidation of both samples are considerably lower than those for sulfite oxidation. This is because the rate of water oxidation on the bare $BiVO_4$ surface is slower than the rate of surface recombination and a considerable fraction of surface-reaching holes is lost to surface recombination.

Supplementary Table 1. Changes in the Bi:V ratio determined by LEIS and work function and VBM determined by XPS of as-prepared and base-treated $BiVO_4$ (010) samples before and after J-V measurement.

As-prepared	Before J-V	After 1 J-V	After 8 J-Vs
Bi:V ratio	43:57	79:21	84:16
Work function (eV)	4.80	4.59	4.36
VBM (eV)	6.38	6.29	6.10

Base-treated	Before J-V	After 1 J-V	After 4 J-Vs
Bi:V ratio	79:21	84:16	86:14
Work function (eV)	4.40	4.40	4.30
VBM (eV)	6.23	6.17	6.06

Supplementary References

1. Park, Y., McDonald, K.J. & Choi, K.-S. Progress in bismuth vanadate photoanodes for use in solar water oxidation. *Chem. Soc. Rev.* **42**, 2321–2337 (2013).
2. Sleight, A.W., Chen, H.-Y., Ferretti, A. & Cox, D.E. Crystal growth and structure of $BiVO_4$. *Mater. Res. Bull.* **14**, 1571–1581 (1979).
3. Wang, W. *et al.* The role of surface oxygen vacancies in $BiVO_4$. *Chem. Mater.* **32**, 2899–2909 (2020).
4. Helander, M.G., Greiner, M.T., Wang, Z.B. & Lu, Z.H. Pitfalls in measuring work function using photoelectron spectroscopy. *Appl. Surf. Sci.* **256**, 2602–2605 (2010).
5. Schäfer, R. & Schmidt, P.C. *Methods in Physical Chemistry* Ch. 15 (Wiley-VCH Verlag GmbH & Co. KGaA, 2012).